Architecture of Clathrin Fullerene Cages Reflects a Geometric Constraint-the Head-to-Tail Exclusion Rule-and a Preference for Asymmetry

ARTICLE *in* JOURNAL OF MOLECULAR BIOLOGY · APRIL 2009

Impact Factor: 4.33 · DOI: 10.1016/j.jmb.2009.01.044 · Source: PubMed

1 AUTHOR:

Stan Schein
University of California, Los Angeles
51 PUBLICATIONS **3,841** CITATIONS

doi:10.1016/j.jmb.2009.01.044 J. Mol. Biol. (2009) 387, 363–375

JMB

Available online at www.sciencedirect.com

ScienceDirect

ELSEVIER

Architecture of Clathrin Fullerene Cages Reflects a Geometric Constraint—the Head-to-Tail Exclusion Rule—and a Preference for Asymmetry

Stan Schein

California NanoSystems Institute, UCLA, Los Angeles, CA 90095-7151, USA

Brain Research Institute, UCLA, Los Angeles, CA 90095-1761, USA

Received 29 March 2008; received in revised form 27 December 2008; accepted 22 January 2009
Available online 29 January 2009

Fullerene cages have n trivalent vertices, 12 pentagonal faces, and $(n-20)/2$ hexagonal faces. The smallest cage in which all of the pentagons are surrounded by hexagons and thus isolated from each other has 60 vertices and is shaped like a soccer ball. The protein clathrin self-assembles into fullerene cages of a variety of sizes and shapes, including smaller ones with adjacent pentagons as well as larger ones, but the variety is limited. To explain the range of clathrin architecture and how these fullerene cages self-assemble, we proposed a hypothesis, the "head-to-tail exclusion rule" (the "Rule"). Of the 5769 small clathrin cage isomers with $n \leq 60$ vertices and adjacent pentagons, the Rule permits just 15, three identified in 1976 and 12 others. A "weak version" of the Rule permits another 99. Based on cryo-electron tomography, Cheng et al. reported six raw clathrin fullerene cages. One was among the three identified in 1976. Here, (1) we identify the remaining five. (2) Four are new and are among the 12 others permitted by the Rule. (3) One, also new, is among the 99 weak version cages. (4) Of particular note, none of the remaining 5565 excluded cages has been identified. These findings provide powerful experimental confirmation of the Rule and the principle on which it is based. (5) Surprisingly, the newly identified clathrin cages are among the least symmetric of those permitted. (6) By devising a method for counting assembly paths, (7) we show that asymmetric cages can be assembled by larger numbers of paths, thus providing a kinetic explanation for the prevalence of asymmetric cages. (8) Finally, we show that operation during cage growth of the Rule greatly increases the likelihood of producing a closed fullerene cage, specifically one of those permitted, but efficient assembly still appears to require internal remodeling.

Keywords: Buckminsterfullerene; endocytosis; self assembly; supramolecular; symmetry

Edited by A. Klug

Introduction

Self assembly of supramolecular structures generally produces a single outcome that is determined either by thermodynamics (least energy) or kinetics (limited pathways). By contrast, trimers ("triskelia") of the protein clathrin self assemble into a variety of fullerene (soccer ball-like) cages with trivalent vertices and faces that are hexagons or pentagons.[1–6] The variety is useful because clathrin cages of many sizes are needed to carry out receptor-mediated endocytosis and protein trafficking at the *trans*-Golgi network.[7–8] Nonetheless, in the face of an infinite number of possible fullerene cages,[9] very few clathrin cages have been identified.[10] Identification of the specific cages that do self assemble and discovery of the rules that underlie those outcomes could provide a general insight into self assembly and clarify the respective roles of thermodynamic and kinetic mechanisms.

Carbon atoms self assemble into a small number of different fullerene cages. The most abundant of these, called Buckminsterfullerene or C_{60}, has the appearance of a soccer ball.[11,12] It is also the smallest

E-mail addresses: schein@ucla.edu; stan.schein@gmail.com.

Abbreviations used: IPR, isolated pentagon rule; DAD, dihedral angle discrepancy.

fullerene cage that obeys the isolated pentagon rule (IPR), wherein every one of the pentagons is surrounded (isolated) by hexagons.[13,14] Carbon atoms self assemble into larger ($n>60$) fullerene cages as well, but only those that obey the IPR,[15–17] and at least one small fullerene cage with 36 vertices, necessarily with adjacent pentagons.[18] The latter cage, shown in Fig. 1 along with its corresponding 2D (Schlegel) graphical representation, is also one that clathrin forms.[10]

Partly on the basis of geometric and energetic considerations and partly on knowledge of those three clathrin and the IPR carbon fullerenes that have been found, we recently proposed a hypothesis, the head-to-tail exclusion rule (the Rule).[19] The Rule excludes self assembly or persistence of cages with faces that would be severely nonplanar,[20] as reviewed below and in more detail in Theory. It accounts for all of the currently known fullerenes and predicts the discovery of only a few others.[19] Specifically, among the 5769 mathematically possible "small" fullerene cage isomers (with $n\leq 60$ vertices and adjacent pentagons),[9] the Rule permits self assembly of just 15 isomers, those shown as Schlegel diagrams in Fig. 2. The three clathrin cages identified in 1976 (28-2, 36-14, and 36-15 in Fig. 2) are among these 15 isomers.[10] (Cage isomers, e.g., 36-15, the 15th isomer with 36 vertices, are numbered in order of production by the pentagon-spiral algorithm.[9,21]) The Rule also permits the soccer ball ($n=60$) and only the very few among large ($n>60$) fullerene cages that obey the IPR.[9,19,22] Many fullerene isomers are chiral, so the 15 of 5769 fullerene isomers corresponds to just 21—the six chiral isomers in Fig. 2 are labeled L&R for left- and right-handed enantiomers—of 11,080 fullerene enantiomers.

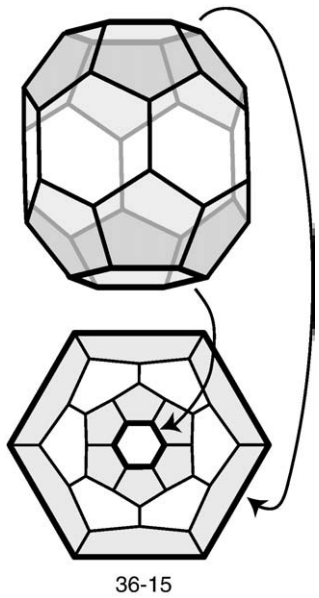

Fig. 1. Fullerene cage 36-15. A fullerene cage has $n\geq 20$ vertices (each connected to three other vertices), $3n/2$ edges, 12 pentagonal faces, and $(n-20)/2$ hexagonal faces, hence $n/2+2$ faces in all. The 3D version of a fullerene cage like 36-15 can be represented by a 2D graph known as a Schlegel diagram.

Recently, eight raw clathrin cage structures were determined by cryo-electron tomography, a method that makes it possible to obtain the 3D structure of individual clathrin cages.[23] Two of the eight (#4 and #1 in Fig. 4B of Ref. 23), have a heptagon and a 13th pentagon and are not fullerenes. The remaining six (#8, #7, #6, #5, #3, and #2) are fullerene cages with $n=36$, 38, 38, 40, 44, and 50 vertices, respectively. For these numbers of vertices, there are 15, 17, 17, 40, 89, and 271 different cage isomers,[9] of which just the 2, 1, 1, 2, 2, and 1 cage isomers shown in Fig. 2 are permitted by the Rule.[19] Many of these cages are chiral, so for these numbers of vertices, there are 23, 30, 30, 66, 162, and 507 different cage enantiomers,[9] of which just the 2, 2, 2, 3, 4, and 1 cage enantiomers shown in Fig. 2 are permitted by the Rule. Thus, if self assembly produced cages at random, the odds against finding just those permitted would be very low indeed. Because one cage, #8, was identified as the permitted 36-14 that had been identified previously,[10] identification of the remaining five raw fullerene cages provides a critical experimental test of the hypothesis.

Here, we identify the five cages, show that four are among those predicted by the Rule, and show that the remainder may be regarded as an exception that proves the rule. Unexpectedly, among the 15 permitted cage isomers (21 permitted cage enantiomers), those identified are the least symmetric. We demonstrate a kinetic explanation for this finding; namely, that more assembly paths lead to self assembly of asymmetric cages. Finally, we apply the insights provided by the Rule to investigate how self assembly is able to find the relatively small number of paths to closed fullerene cages.

Results

Identification of the new, raw clathrin cages

Two of the raw fullerene cages with 38 vertices, #7 and #6, are mirror images, left- and right-handed version of the same cage, so it will be enough to identify one of them. A view of each of the four remaining unidentified cage structures, reproduced from the published Fig. 4B of Ref. 23, is shown at the far right in each of the parts (a–d) of Fig. 3. We took advantage of a variety of clues to identify these.[19] For example, the Rule permits just one cage (38-17) with 38 vertices, and that comes in left- and right-handed versions, so 38-17 was a first guess for the identity of the published #7 structure at the far right in Fig. 3a. Also, the published structure shows a hexagon surrounded by five pentagons and one hexagon, another feature consistent with 38-17. These and similar features, including strings and rings of pentagons and hexagons, are most easily appreciated in the four Schlegel diagrams shown at the far left in each of the parts (a–d) of Fig. 3. Nonetheless, we used the most

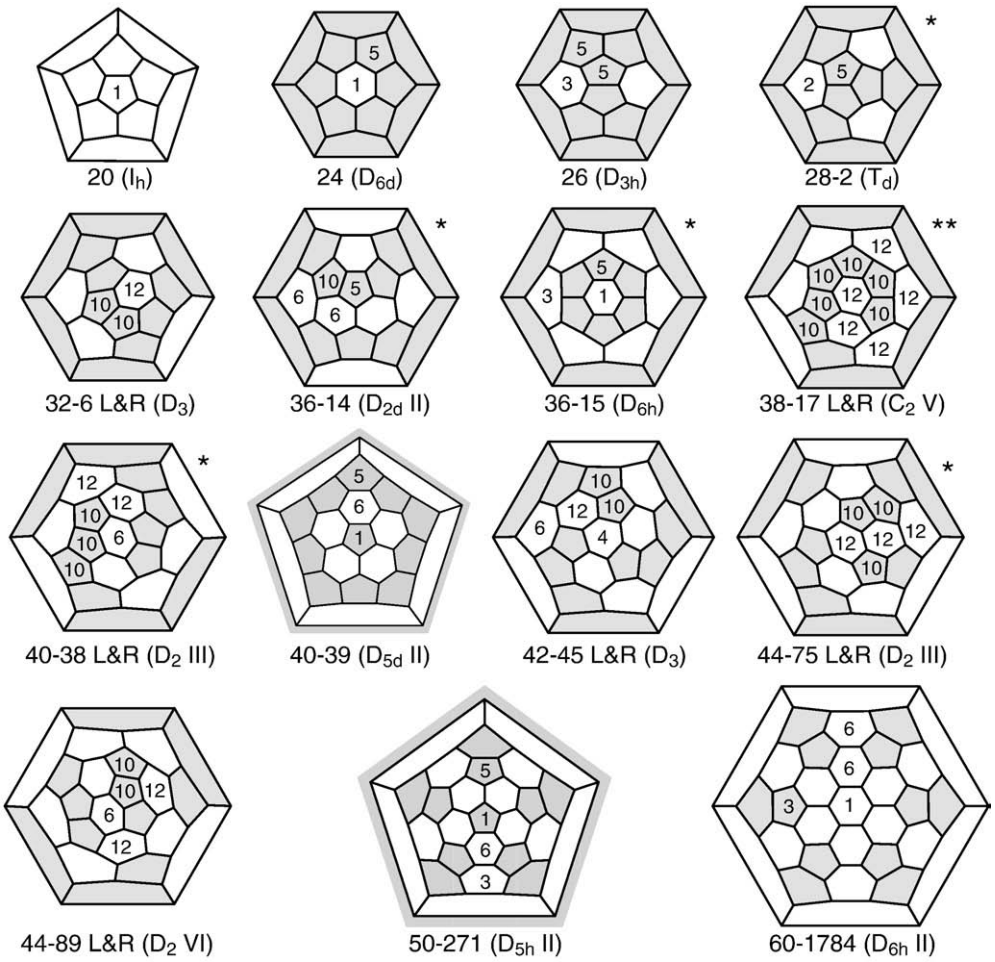

Fig. 2. Small fullerene cages permitted by the Rule. There are 15 small ($n \leq 60$) fullerene cage isomers—but 21 cage enantiomers since chiral versions (L and R) are counted as two—with adjacent pentagons that obey the head-to-tail exclusion rule. The faces with numbers inside them are non-equivalent, and each number shows how many different spiral assembly paths originate from that face. Cages with an asterisk (*) were identified earlier or in this study. Cages are numbered in order of production by the pentagon-spiral algorithm,[9,21] and the point group is in Schoenflies notation.

rigorous method of identification; namely, sequentially numbering each vertex of the published structures (rightmost pictures) while drawing and numbering the corresponding Schlegel diagrams (leftmost). The process was assisted by access to a version of Fig. 4B of Ref. 23 without the occluding vesicles that are in the published figure (Y. Cheng *et al.*, personal communication).

We then compared the Schlegel diagrams so drawn and numbered (leftmost in Fig. 2a and b) to the Schlegel diagrams of all of the cage isomers 17, 40, 89, and 271 with 38, 40, 44, and 50 vertices, which we produced with the CaGe program.[24] In each case, the 3D view of each identified cage, as shown by the stereopairs in the center parts of Fig. 3a–d, closely resembles the published picture (rightmost in Fig. 3a–d) and the picture without the occluding vesicles.

The chiral cage in Fig. 3a with 38 vertices, a string of 12 pentagons and a string of 9 hexagons, is indeed the predicted 38-17 (Fig. 2). The cage in Fig. 3b with 40 vertices and two strings of six pentagons is 40-38, one of the two isomers with 40 vertices predicted by the Rule (Fig. 2). The cage in Fig. 3c with 44 vertices, two strings of four pentagons, and two strings of two pentagons, is 44-75, one of two predicted isomers with 44 vertices (Fig. 2). However, the cage in Fig. 3d with 50 vertices and six pentagon doublets is 50-270, not the predicted isomer with 50 vertices, 50-271 (Fig. 2).[19] Nonetheless, as we describe next, 50-270 is an exception that proves the rule.

An exception that proves the Rule

The physical mechanism of the Rule can be understood at the level of the Ring, a center (pentagonal or hexagonal) face and its five or six surrounding (or external) faces, as described further in Theory.[20] Several Rings are shown in Fig. 4a. The Rule would exclude from self assembly Rings with (colored) vectors arranged head of one to tail of another; for example, Rings 631, 521 and 632 in Fig. 4a.

As shown in Fig. 4b, each colored vector may be drawn for a particular arrangement of four

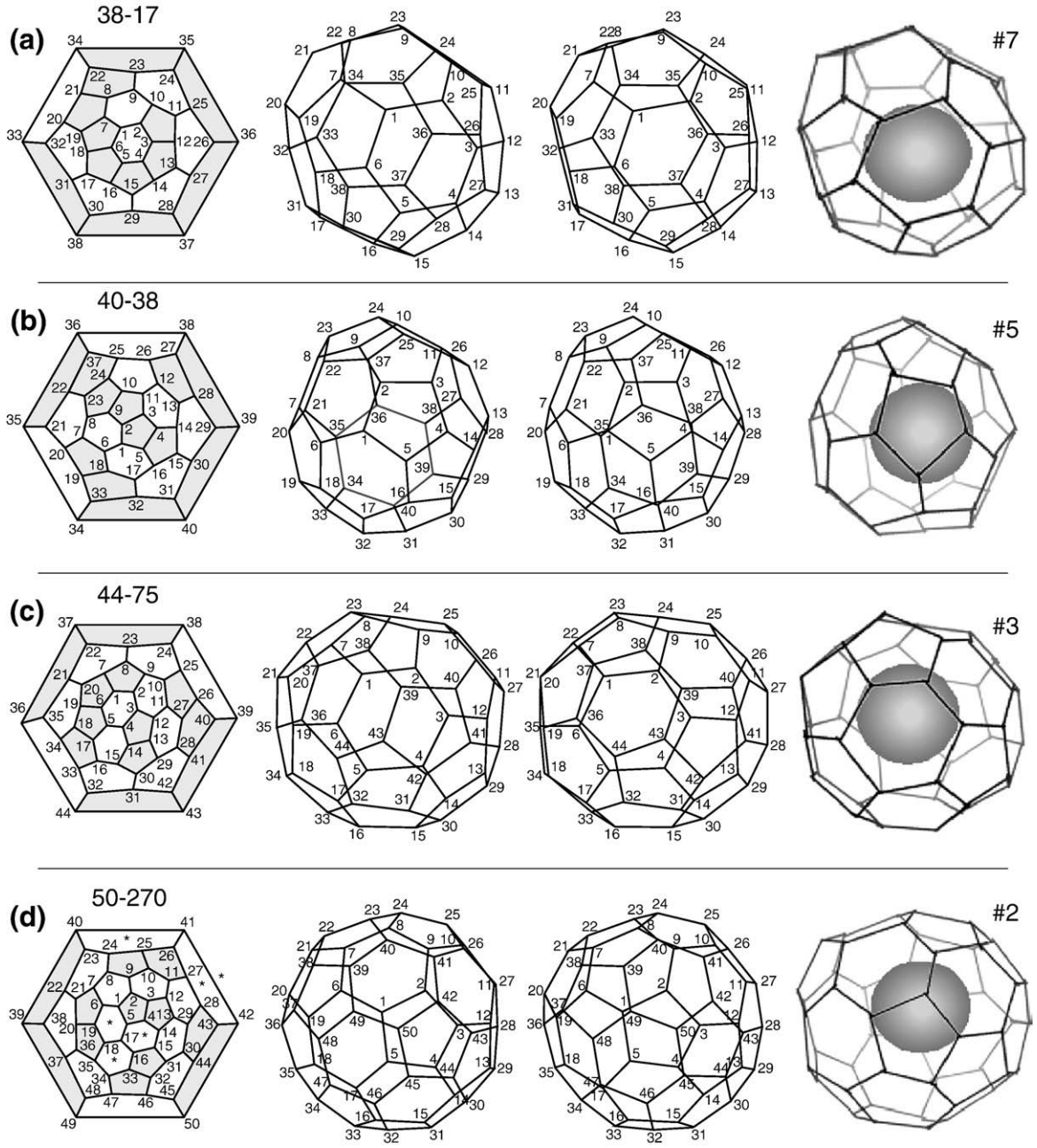

Fig. 3. Identification of new clathrin fullerene cages. Each part (a–d) shows the published view of a cage from Ref. 23 at the far right, the corresponding 3D stereopair in the middle with numbered vertices, and the corresponding Schlegel diagram at the far left, also with numbered vertices. a, #7 from Fig. 4B of Ref. 23; cage 38-17. b. #5 from Fig. 4B of Ref. 23; cage 40-38. c. #3 from Fig. 4B of Ref. 23; cage 44-75. d. #2 from Fig. 4B of Ref. 23; cage 50-270. Asterisks (∗) mark hex-rings 632.

(hexagonal and pentagonal) faces, specifically the three arrangements that have a pentagon at one end of the colored edge and a hexagon at the other. In each of these three (green, red, and blue) arrangements, the dihedral angle about the colored edge at its pentagon end is different (and smaller) than the dihedral angle about the colored edge at its hexagon end. We call this difference a dihedral angle discrepancy (DAD).

Figure 4c details why the dihedral angles about an edge with a green DAD are different: The vertex at the right-hand end of edge 12, the edge with the green DAD vector, joins a pentagon and two hexagons. The dihedral angle about this edge at its pentagon end on the right, the angle between the two shaded planes, is 138.2°. The vertex on the left joins three hexagons, so the dihedral angle about this edge at its hexagon end, the angle between a different pair of shaded planes, is 180°. The green DAD vector thus denotes a dihedral angle discrepancy of 41.8°, pointing in the direction of the increase from right (138.2°) to left (180°).

Because the two dihedral angles are different, as shown in stereo in Fig. 4d, one or generally both of

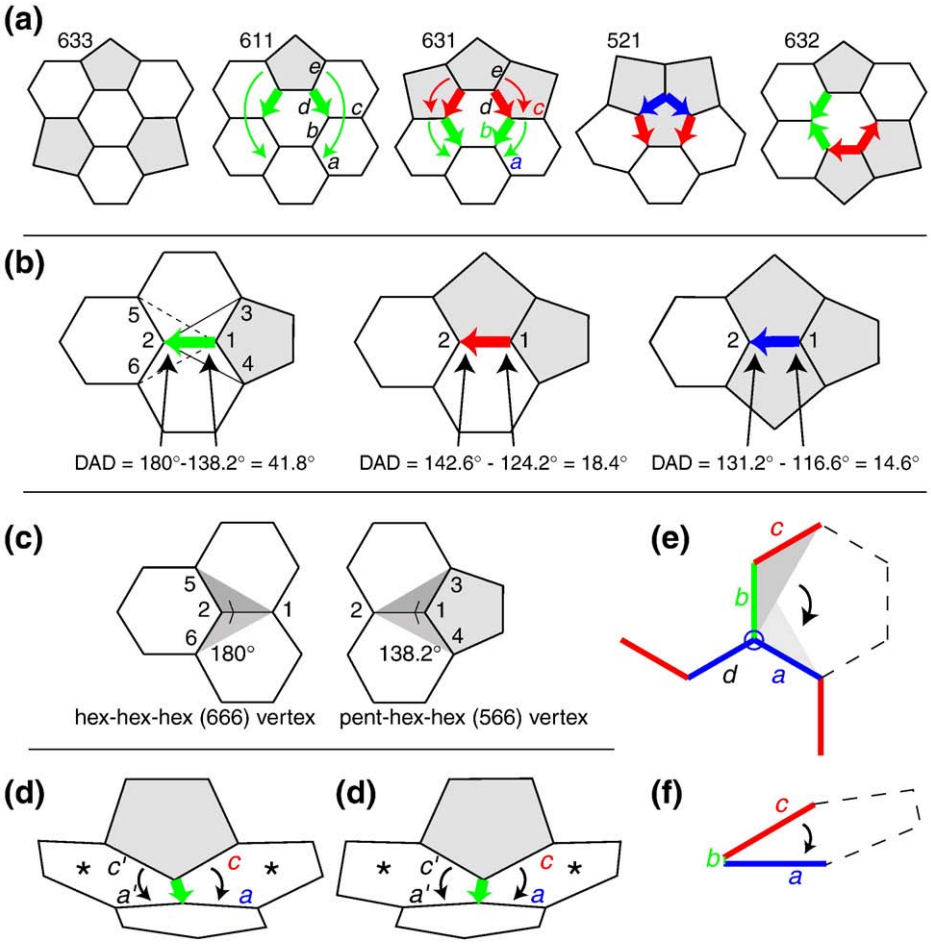

Fig. 4. DADs and the Rule. (a) Four of the 13 hexagon-centered rings and one of the eight pentagon-centered rings. The numbering of the eight pentagon-centered and 13 hexagon-centered rings is described in Ref. 19. (b) Three types of dihedral angle discrepancy (DAD). (c) Different dihedral angles at the pentagon (566) end and the hexagon (666) end of edge 12. (d) Stereo view showing a larger (flatter) dihedral angle about the green edge at its hexagon end than at its (raised) pentagon end, holding *a* and *a′* edges below *c* and *c′* edges and making the side hexagons (asterisks) nonplanar. (e) Clathrin triskelion with a central hub (circled vertex), three proximal legs (edges *a, b,*and *d*) and three distal legs (e.g., edge *c*). If edge *a* is rotated about edge *b* down from edge *c*, the (broken line) presumptive hexagonal face is nonplanar. (f) The nonplanarity of the broken linehexagonal face in e can be appreciated by sighting along edge *b*.

the faces (marked with asterisks) to the sides of the edge marked with the colored DAD vector must be nonplanar.

As described in Theory, a pair of DADs in a head-to-tail arrangement, which can be seen on both sides of Ring 631 in Fig. 4a, would make the faces external to those four DAD edges in Ring 631 severely nonplanar.[20] (By comparison, a single DAD on each side, as in Ring 611 in Fig. 4a, causes much less severe nonplanarity among the surrounding faces.[20]) The group of faces that constitute Ring 631 would therefore be unlikely to self assemble, and if Ring 631 did assemble, it would be unlikely to persist. Ring 631 would thus be an "improbable Ring".[19,20] Four of the 13 hexagon-centered Rings and two of the eight pentagon-centered Rings have head-to-tail DADs and are designated as improbable Rings.[19]

Correspondingly, a cage with a Ring-631 arrangement of faces, for example, would be unlikely to self assemble or to persist, and that cage would be improbable. The Rule predicts that no cage with any of these six improbable Rings would self assemble.

Five of the six improbable Rings are like Ring 631 in having two sets of head-to-tail DADs, one set on each side. However, Ring 632 in Fig. 4a has just one set and might not be quite so improbable. We therefore speculated that cages with the 632 type of Ring but none of the other five types of improbable Ring might be rare, but not as rare as cages with any of the other five types of improbable Ring.[19] By allowing Ring 632, the weak version of the Rule would permit 99 additional cage isomers for $n \leq 60$, including 10 of the 271 cage isomers with 50 vertices.[19]

The new fullerene cage with 50 vertices, 50-270 (Fig. 3d) is one of the weak version cages. Thus, the six clathrin fullerenes in Fig. 4B of Ref. 23 include five of the 15 cage isomers (21 cage enantiomers) permitted by the Rule for $n \leq 60$, one of the 99 cage isomers permitted by the weak version of the Rule, and none of the 5565 remaining cage isomers. As

speculated,[19] weak version cages are relatively improbable but not impossible.

The new cages are among the most asymmetric

The three isomers identified in 1976, 28-2, 36-14 and 36-15 in Fig. 2,[10] may have been identified because of their symmetry and consequent ease of inferring those structures from views of many cages in electron micrographs. The six cage structures reported recently,[23] which include 36-14, are likely to be a more representative sample, since cryo-electron tomography can provide the 3D structure of individual, randomly selected cages. Unexpectedly, given that the carbon Buckminsterfullerene and spherical viruses self assemble into icosahedral (I_h) cages [11,25–27] with the highest possible symmetry order, 120,[9] the six clathrin fullerene cages are among the least symmetric of the permitted cages.

In Fig. 5a, the symmetry orders of the observed cages are represented by filled symbols. Two of the six are 38-17, the left- and right-handed versions, the least symmetric (C_2 symmetry, with symmetry order 2) of all of the permitted cages. One is 36-14 (D_{2d} symmetry, with symmetry order 8); by contrast, the other permitted cage with 36 vertices, 36-15, would have had D_{6h} symmetry and symmetry order 24, three times as great. One is 40-38 (D_2 symmetry, symmetry order 4); by contrast, the other permitted cage with 40 vertices, 40-39, would have had D_{5h} symmetry and symmetry order 20, five times as great. One is the weak Rule cage 50-270 (D_3 symmetry, symmetry order 6); by contrast, the strict Rule cages with 50 vertices, 50-271, would

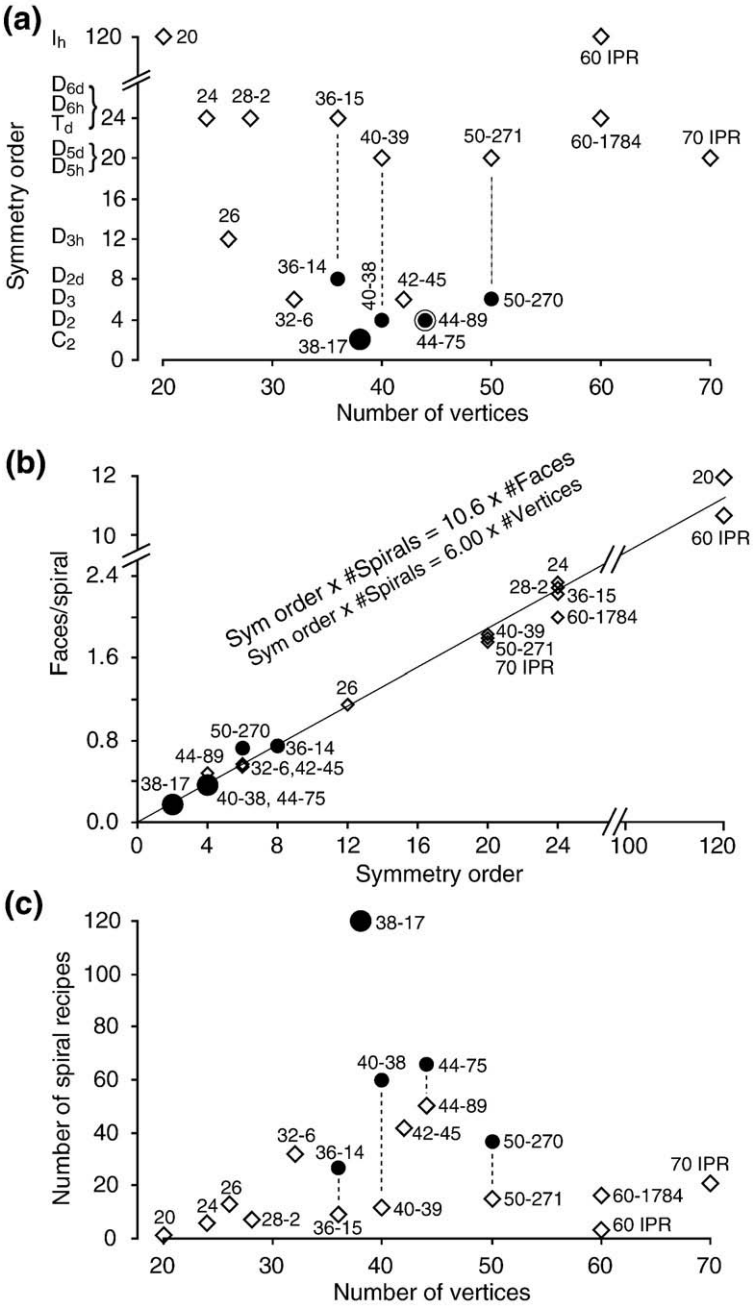

Fig. 5. The identified cages are less symmetric than the other permitted cages, corresponding to a larger number of spiral assembly paths. (a) Symmetry order of newly identified cages (filled circles) from Ref. 23, including the two identified versions of the chiral cage 38-17 (large, filled circle), plus other cages permitted by the Rule, including the IPR cages with 60 and 70 vertices (open diamonds). Because of overlap, permitted cage 44-89 is represented by a large open circle. (b) Inverse proportionality between spirals/face and symmetry order. The coefficient of determination (R^2) of the line, $(\text{spirals/face})^{-1}$ *versus* symmetry order, is 0.9947. A similar figure could be drawn to show inverse proportionality between spirals/vertex and symmetry order. The R^2 of the corresponding line $(\text{spirals/vertex})^{-1}$ *versus* symmetry order, is 0.9996. c, Number of spiral paths for the cages listed in A; same symbols as in a. Dotted lines point between cages with the same number of vertices, with one newly found and the other not.

have had D_{5h} symmetry and symmetry order 20, over three times as great. Only the symmetry order of the one observed cage with 44 vertices, 44-75 (D_2 symmetry, symmetry order 4) is not less than that of the other permitted cage, 44-89; in this case, the two permitted cages have the same symmetry and thus the same symmetry order.

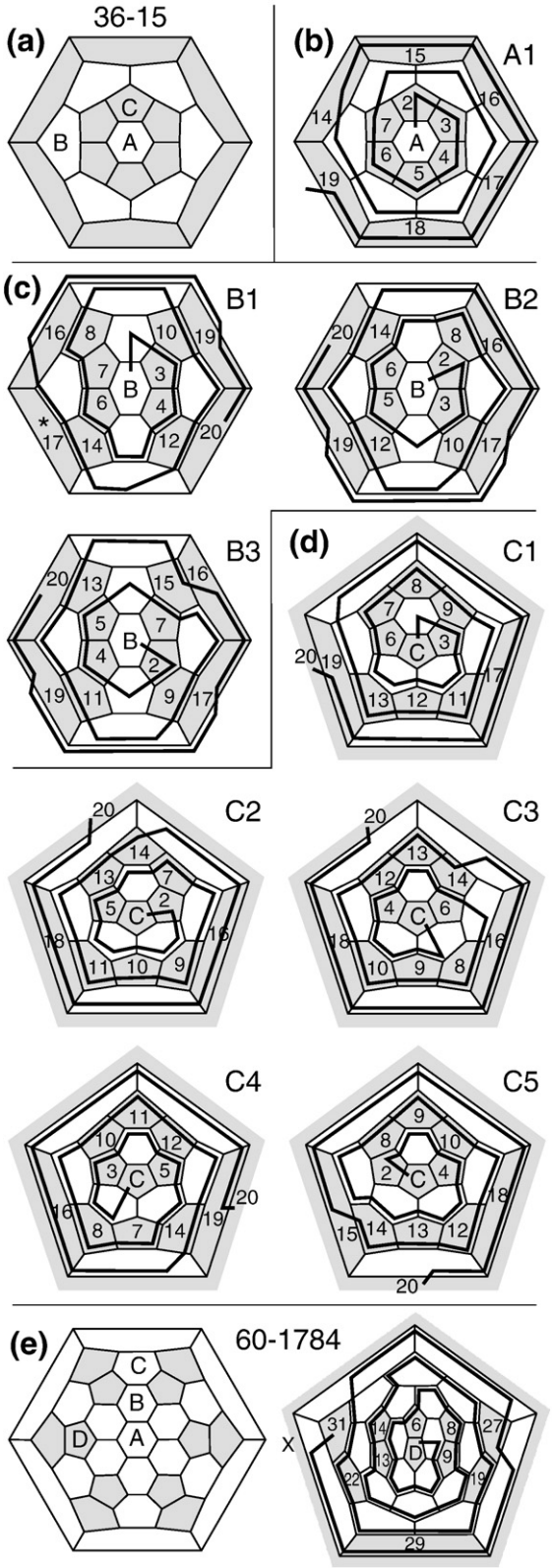

Fig. 6. All spiral paths to cage 36-15 and a failed path to 60-1784. (a) Three non-equivalent faces (A, B, and C) in cage 36-15. (b) Numbering of the 12 pentagons along the one non-equivalent spiral path originating from face A. (c) Numbering of pentagons along the three non-equivalent spiral paths from face B. For the first successful path, completion of face 16 also completes face 17 (asterisk) even though the spiral bypasses face 17. (d) Numbering of pentagons along the five non-equivalent spiral paths from face C. (e) Four non-equivalent faces (A–D) in 60-1784. This path from face D is an example of one that fails to assemble a face, the one marked by x. See the text for further explanation.

Number of spiral assembly paths is inversely proportional to symmetry order

We wondered if greater symmetry reduced the number of paths to assembly of a cage. As can be appreciated from the 3D structure of 36-15 and its Schlegel diagram (Fig. 1), the two isolated (floor and ceiling) hexagons are equivalent by symmetry. In Fig. 6a, we label that face A. Similarly, all of the hexagons in the ring of six hexagons are equivalent by symmetry (the B face in Fig. 6a), as are all of the 12 pentagons (the C face in Fig. 6a). (Equivalence in these cases is due to both mirror and rotational symmetry.) Thus, even though 36-15 has 20 faces, for the purpose of generating a complete list of assembly paths, we need consider only the paths that originate from those three non-equivalent faces A, B, and C. (By contrast, the comparatively asymmetric 38-17, with 21 faces, has 11 non-equivalent faces.) Because cage 36-15 has only three non-equivalent faces, it is helpful to portray it by three different Schlegel diagrams, one centered on face A (Fig. 6b), another centered on face B (Fig. 6c), and a third centered on face C (Fig. 6d). These different Schlegel diagrams are useful for drawing all of the assembly paths that originate from each face.

Spiral paths are convenient to list and then count assembly paths, even though addition of vertices and assembly of new faces is likely to occur at the entire rim of a growing cage.[9,21] Consider the spiral path that originates from face A in Fig. 6b. The order of the 20 faces along that spiral path, a "spiral recipe", is 65555556666665555556, a 20-digit "binary" number but with 5 and 6 instead of 0 and 1. Even though a hexagon could be the origin of 12 spiral paths, six clockwise and six counter-clockwise, due to mirror and rotational symmetry all of the spiral paths that originate from hexagonal face A in 36-15 (Fig. 6b) would have this same recipe. All of the paths are thus identical, and we can obtain only one spiral recipe by starting with face A. Similarly, only three (out of potentially 12) spiral paths that originate from hexagonal face B are non-equivalent (Fig. 6c), and only five (out of

potentially 10) spiral paths that originate from pentagonal face C are non-equivalent (Fig. 6d).

Here is the list of recipes for the nine spiral paths (one from A, three from B, and five from C) that produce cage 36-15:

A1: 65555556666665555556
B1: 66556555656565655655
B2: 65565565656565655655
B3: 65655656565656555655
C1: 56566555565556665655
C2: 55665656555655656565
C3: 56656565556555656565
C4: 56565655655565656655
C5: 55656665556555566565

Because the origin and end of each spiral path are non-contiguous faces, such spiral recipes do not circularly permute and cannot be reversed to generate new recipes that would produce 36-15. (However, the A1 recipe can be reversed, because doing so produces the same 20 digit recipe, not a new one.) Therefore, these nine spiral paths, encoded by the 20 digit binary recipes listed above, are the only ones that produce 36-15.

The first path (B1) in Fig. 6c appears to miss face #17 (marked with an asterisk); however, addition of the vertices that complete face #16 also completes the "missed" face #17. Thus, as can be confirmed by drawing faces in the order listed above for B1, this path is successful in generating a Schlegel diagram that corresponds to 36-15. However, as shown in Fig. 6e, one path that originates from the D face of 60-1784 also appears to miss a face (marked with an x), but in this case, drawing the faces according to the spiral recipe fails even to reproduce a closed cage, much less 60-1784. Therefore, to obtain a complete listing of spiral recipes, we had to draw every potential spiral path and check if any faces appeared to be missed.

By drawing and then counting all of the spiral paths for 18 cages (the 15 small, non-IPR cage isomers permitted by the Rule, 50-270, and the IPR cages with 60 and 70 vertices), we could test the hypothesis that the number of spiral paths is inversely proportional to symmetry order. The numbers in the faces of the Schlegel diagrams in Fig. 2 are the number of non-equivalent spiral paths originating from each of the non-equivalent faces for the 15 small, non-IPR cage isomers permitted by the Rule. Taking the total number of faces in each cage into account, the data in Fig. 5b show an excellent linear fit of $(\text{spirals/face})^{-1}$ to symmetry order—expressed by the equation on the graph—and confirm the hypothesis: asymmetric cages do have more assembly paths.

Taking the total number of vertices instead of the number of faces in each cage into account, a figure like Fig. 5b (not shown) also shows an excellent linear fit of $(\text{spirals/vertex})^{-1}$ to symmetry order, expressed by the equation that is shown in smaller type in the graph in Fig. 5b.

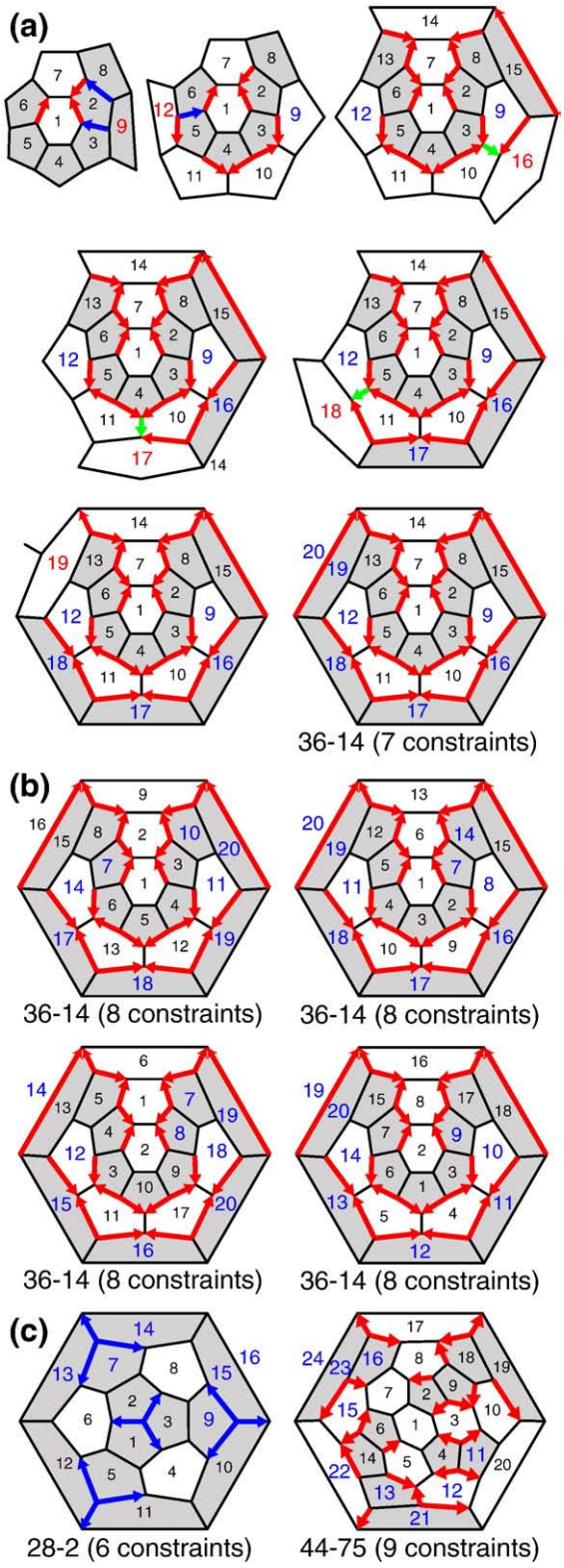

Fig. 7. The Rule constrains the choice of many faces along a spiral assembly path. (a) Seven faces constrained for this spiral path to 36-14. Five wrong choices of face due to production of head-to-tail DADs are marked by large red numerals; their replacement faces are marked by large blue numerals. (b) Totals of eight, nine, nine, and eight faces constrained for four other spiral paths to 36-14. (c) Six constrained faces for this spiral path to 28-2, and nine constrained faces for this spiral path to 44-75.

Correspondingly, Fig. 5c shows that in every case, the six fullerene cages reported in Ref. 23 and identified here have either the largest number of spiral paths overall (38-17) or the larger number between the two cages that are permitted for each $n = 36$, 40, 44, and 50 vertices.

Operation of the Rule during self assembly

If cages grew by random addition of hexagons and pentagons, then the number of possible outcomes with 20 faces, as in a cage with 36 vertices, would be:

$$2^{20} = 1,048,576$$

By contrast, only 15 cage isomers with 36 vertices are possible,[9,21] and only two of those would be permitted by the Rule. Consider for example the probability of growing 36-14, the more likely of the two permitted cage isomers with 36 vertices, by random addition of faces. With 27 spiral recipes producing 36-14 (Fig. 2), the probability of growing 36-14 would be:

$$27/1,048,576 = .0025\%$$

However, if addition of faces that would result in a head-to-tail DAD could not occur for geometric reasons,[20] then addition of hexagonal and pentagonal faces would not be entirely random. We called such a constraint on the type of face to be added during growth the probable roads hypothesis.[19]

Figure 7a focuses on one spiral path to 36-14. Either a pentagon or a hexagon would be permitted at each of faces #1 through #8. Assuming that the "correct" faces (to make 36-14) had been chosen for those faces, a pentagon at face #9 would create a head-to-tail DAD. Therefore, face #9 is constrained to be a hexagon. A "wrong" choice for each of five of the 20 faces (#9, #12, #16, #17, and #18) would create a head-to-tail DAD; only one choice for the penultimate face (#19) closes the cage; and the ultimate face (#20) is determined by what is left after closure by the penultimate face. Thus, seven of the 20 faces are constrained to be the hexagon or pentagon that is the correct choice from the point of view of assembling 36-14. In the last diagram in Fig. 7a, the seven constrained faces are marked with large, blue numbers. In Fig. 7b, the diagrams show eight, nine, nine, and eight constrained faces for four more spiral paths to 36-14, showing that the number of constrained faces depends, to some extent, on the path. Figure 7c shows six constrained faces for one spiral path of 16 faces to grow 28-2. It also shows nine constrained faces for one spiral path of 24 faces to grow 44-75.

Four faces are required to produce a single DAD (Fig. 4d); at least five are required to produce the two DADs of a head-to-tail DAD. Therefore, subtracting 4 from the 16, 20, and 24 faces in 28-2, 36-14, and 44-75 gives the numbers 12, 16, and 20 of faces that could be constrained. Of these, approximately six, eight and nine, or ~50%, are constrained, reducing the number of possible outcomes by approximately 2^6, 2^8 and 2^9 (64-, 256- and 512-fold) and increasing the probability of self assembly of these cages by the

Table 1. Probability of self assembly of permitted cage enantiomers along constrained spiral paths

Isomer	Point Group	Sym order	Faces	Constr faces	Unconstr faces	Outcomes	Good spirals	Prob success (%)	Prob∗ success (%)	Prob failure 84.12%
20-1	I_h	120	12	4	8	256	1	0.39	0.39	99.61
24-1	D_{6d}	24	14	5	9	512	6	1.17	1.18	98.82
26-1	D_{3h}	12	15	5.5	9.5	724	13	1.80	1.82	98.18
28-2	T_d	24	16	6	10	1024	7	0.68	0.71	99.29
32-6L	D_3	6	18	7	11	2048	32	1.56	1.63	98.37
32-6R	D_3	6	18	7	11	2048	32	1.56	1.63	98.37
36-14	**D_{2d}**	**8**	**20**	**8**	**12**	**4096**	**27**	**0.66**	**0.70**	**99.30**
36-15	D_{6h}	24	20	8	12	4096	9	0.22	0.23	99.77
38-17L	**C_2**	**2**	**21**	**8.5**	**12.5**	**5793**	**120**	**2.07**	**2.22**	**97.78**
38-17R	**C_2**	**2**	**21**	**8.5**	**12.5**	**5793**	**120**	**2.07**	**2.22**	**97.78**
40-38L	**D_2**	**4**	**22**	**9**	**13**	**8192**	**60**	**0.73**	**0.82**	**99.18**
40-38R	D_2	4	22	9	13	8192	60	0.73	0.82	99.18
40-39	D_{5d}	20	22	9	13	8192	12	0.15	0.16	99.84
42-45L	D_3	6	23	9.5	13.5	11,585	42	0.36	0.41	99.59
42-45R	D_3	6	23	9.5	13.5	11,585	42	0.36	0.41	99.59
44-75L	**D_2**	**4**	**24**	**10**	**14**	**16,384**	**66**	**0.40**	**0.46**	**99.54**
44-75R	D_2	4	24	10	14	16,384	66	0.40	0.46	99.54
44-89L	D_2	4	24	10	14	16,384	50	0.31	0.35	99.65
44-89R	D_2	4	24	10	14	16,384	50	0.31	0.35	99.65
50-270L	**D_3**	**6**	**27**	**11.5**	**15.5**	**46,341**	**37**	**0.08**	**0.09**	**99.91**
50-270R	D_3	6	27	11.5	15.5	46,341	37	0.08	0.09	99.91
50-271	D_{5h}	20	27	11.5	15.5	46,341	15	0.03	0.04	99.96
60-1784	D_{6h}	24	32	14	18	262,144	16	0.01	0.01	99.99

Bold-face rows of numbers correspond to the newly identified cages. As described in the text, failure to achieve one of the good spirals with n vertices reduces the number of potential spirals for larger cages ("outcomes"), thus increasing slightly the probability of generating one of the longer successful spirals. The probabilities in the column (Prob∗) take this reasoning into account.

same factors. Actually, the increase in probability is slightly greater: If constrained self assembly failed to produce the 20-1 cage (555555555555), all of the random spiral paths that began with those 12 digits would be eliminated from the group of possible outcomes of further growth. Likewise, if further assembly failed to produce the 24-1 cage, all of the random paths that began with any of the six 14-digit spiral recipes that would produce 24-1 (65555555555556, 56555555556555, etc.) would also be eliminated from the group of possible outcomes of further growth.

On the basis of this reasoning and assuming that the number of constrained faces equals (number of faces − 4)/2, Table 1 shows the probability of constrained self assembly of each the 21 small cage enantiomers with adjacent pentagons permitted by the Rule plus the two enantiomers of 50-270. Table 1 shows also that the probability for 36-14, for example, is 0.70%, a factor of 271 (slightly more than 256) greater than if assembly was completely random. The probability that constrained self assembly would fail to produce 36-14 is thus:

$$100\% - 0.70\% = 99.30\%$$

The probability that constrained self assembly would fail to produce any of these 23 cage enantiomers is 84.1%, the product of the probabilities of failure of each of the 23. Therefore, the data predict that constrained assembly would produce closed small fullerene cages with adjacent pentagons—specifically those permitted by the Rule—from 16% of starts.

To test this prediction, we simulated growth of fullerenes by adding faces along a spiral path, the choice of each additional face chosen by a random number generator but changed if that choice would produce head-to-tail DADs. For 30 trials, two (7%) produced large IPR fullerenes. Six (20%) produced small fullerenes (one 24-1, one 26-1, two 28-2, and two 36-14), not far from the predicted 16%. Thus, constrained self assembly might explain self assembly of fullerene cages from purified clathrin protein *in vitro*.[28] However, these probabilities are still quite low, so assembly constrained by the Rule is unlikely to provide a full explanation of self assembly *in vivo*, which must be far more efficient.

Discussion

New clathrin fullerene cages confirm the Rule

Of the 5770 mathematically possible cages with $n \leq 60$ vertices, one is the soccer ball with isolated pentagons, leaving 5769 with adjacent pentagons. With 15 cage isomers that obey the strict version of the Rule and 99 that obey the weak version of the Rule, 5655 small cages with adjacent pentagons are excluded. Not one of this last group of 5655 has been observed, a powerful experimental confirmation of the Rule.

Moreover, for $n \leq 60$ the new tally—six observed non-IPR cage isomers (asterisks in Fig. 2) of 15 cage isomers (or seven observed non-IPR cage enantiomers of 21 cage enantiomers) that obey the strict version of the Rule and one of the 99 cage isomers that obey the weak version of the Rule—reveals a strong predominance of the strict version cages. The one exceptional cage, 50-270, shows that it is possible for a Ring with one set of head-to-tail DADs to self assemble—and thus possible for a cage with head-to-tail DADs to self assemble—but these weak version cages appear to be far less probable than Rings without any head-to-tail DADs, consistent with the logic of the Rule.[19] The weak version 50-270 cage isomer is thus an exception that proves the rule.

Thermodynamics and kinetics

Individual clathrin triskelia may enforce the Rule during self assembly of fullerene cages because of the presence of distal legs (e.g., edge *c* in the clathrin triskelion shown in Fig. 4e) that are each unable to rotate far out of the plane formed by its non-adjacent proximal leg (e.g., edge *a*) and its adjoining proximal leg (e.g., edge *b*). Without operation of the Rule, the number of outcomes for random addition of faces would be undiminished. For example, of 2^{20} possible outcomes for a cage with 36 vertices and 20 faces, only 23 enantiomers[9] would be closed cages, and only two of those would be permitted cages. Thus, it should be no surprise that triskelia without distal legs generally fail to assemble closed cages.[29]

Severe torsion of the adjoining proximal leg (e.g., *b* in Fig. 4e) associated with a head-to-tail arrangement of DADs would incur a large energy cost, so excluded cages would be disfavored in an equilibrium situation. However, except for the dodecahedron ($n = 20$) and the soccer ball ($n = 60$), all of the clathrin cages permitted by the Rule do have $^{\text{DADs}}$[19] and torsion, though less and at a smaller energy cost. Of particular note, a lower number of DADs does not explain why asymmetric cages are favored. Specifically, the identified 36-14 has 24 red DADs; so does 36-15. The identified 44-75 has 24 red DADs; 44-89 would have fewer red DADs, just 16, not more. The identified 40-38 has 24 red DADs; 40-39 would also have fewer, just 20. And, the doubly identified 38-17 has 24 red DADs.[19] Therefore, instead of an equilibrium-thermodynamic explanation based on energy, we suggest that asymmetric cages are favored for the kinetic reason documented here, that more assembly paths lead to asymmetric cages. Indeed, both the experimental finding that asymmetric cages are favored and the explanation in terms of numbers of assembly paths suggest that we might not see many more than the six already observed fullerene cage isomers of the 15 permitted by the Rule or many more than the seven already observed clathrin fullerene cage enantiomers of the 21 permitted by the Rule.

Carbon fullerenes are consistent with the Rule but favor symmetric cages

Carbon atoms self assemble into the same small non-IPR isomer 36-15 formed by clathrin.[18] Cages with 32, 44, and 50 carbon atoms have been noted—possibly the isomers 32-6, 44-75, 44-89 and 50-271 that are predicted by the strict version of the Rule[19]—but the specific isomers were not identified.[30,31] Other than 36-15[18] and Buckminsterfullerene ($n=60$),[11,12] all of the other empty carbon fullerenes that have been identified are large ($n>60$) and obey the IPR.[15–17] Correspondingly, the strict version of the Rule permits 36-15 among the small ($n\leq 60$) non-IPR cages, Buckminsterfullerene ($n=60$), and only IPR cages for $n>60$.[19,22] For carbon, the evidence is thus consistent with the strict version of the Rule. In that case, we suggest that enforcement of the Rule by carbon fullerenes is accomplished locally by the presence of double and intermediate bonds that discourage the severe nonplanarity associated with head-to-tail DADs.[22]

However, whereas clathrin favors asymmetric cages, the most abundant carbon fullerene cage is the icosahedral Buckminsterfullerene with the highest symmetry order, 120.[9] The second most abundant carbon fullerene cage is the D_{5h} IPR isomer of C_{70},[15] also with high symmetry order, 20.[9] Although both clathrin and carbon cages obey the Rule, this difference suggests that the processes of fullerene assembly by clathrin protein and by carbon atoms are fundamentally different. Indeed, the currently favored process for assembly of Buckminsterfullerene and the IPR isomer of C_{70} involves shrinkage from giant fullerenes by loss of carbon dimers,[32–36] a process explained by a kinetic mechanism.[37]

Efficient assembly

We showed that random self assembly constrained by the Rule has a probability of ~16% for producing closed small fullerene cages with adjacent pentagons. What mechanisms might enable more efficient self assembly of clathrin cages *in vivo*? Here is one possible mechanism: it is likely that when a cage grows over a template, like a spherical vesicle of a particular diameter, the cage may accumulate curvature-generating pentagons at the density required to achieve the appropriate diameter cage, perhaps assisted by adapter proteins.[7,29,38] Indeed, merely specifying that a cage with 36 vertices will have 12 pentagons (and thus 8 hexagons) among its 20 faces reduces the number of random outcomes from 2^{20} to $20!/(12!\times 8!)$, an eightfold reduction.[19,21] Here is another possible mechanism: assembly along what would have been a failed path to a fullerene (e.g., see Fig. 3A of Ref. 19) might be rescued by completion of a heptagonal or larger face at the very end. Indeed, two of the eight newly reported cages[23] have a heptagon (and a 13th pentagon). Although such outcomes are not fullerenes, they are closed clathrin cages.

Nonetheless, it seems clear that editing of face type to eliminate head-to-tail DADs is likely to occur internally as well as at the rim of a growing clathrin cage.[39–43] Such a suggestion is consistent with the finding that clathrin protein can exchange between apparently complete cages and the cytoplasm.[44–46] For carbon fullerenes, the fullerene-road hypothesis[47,48] and the shrinking hot giant hypothesis[34–37] similarly require remodeling[9] of complete cages to eliminate adjacent pentagons and generate IPR fullerenes. However, the growth and editing mechanisms operate, the Rule is a geometric constraint that promotes successful self assembly by greatly limiting the number of outcomes, and the final products of self assembly from both clathrin protein and from carbon atoms are consistent with the Rule.

Theory

Dihedral angle discrepancy (DAD)

Each clathrin triskelion in a clathrin fullerene cage provides a vertex (circle in Fig. 4e) and contributes three proximal edges (*a*, *b*, and *d*) that connect to three adjacent vertices. Likewise, each carbon atom in a carbon fullerene cage is a vertex and contributes three edges (e.g., two single bonds and one double bond) that connect to three adjacent vertices.

In a fullerene cage, an edge with a pentagon at one end and a hexagon at the other has nonplanar faces to its sides. In the case of the green edge in stereo Fig. 4d,[20] the *a* and *a′* edges at the hexagon end of the green edge are rotated down from the *c* and *c′* edges at the pentagon end of the green edge, so one or generally both of the side hexagons (marked by asterisks) are nonplanar.

The cause of these rotations is explained in Fig. 4c. In the left-hand diagram, the vertex joining three hexagons (6gons) is a 666 vertex. The dihedral angle about edge 12 at its 666 end, that is, the angle between the two shaded planes, is 180°. In the right-hand diagram, the dihedral angle about edge 12 at its 566 end, that is, the angle between those two shaded planes, is 138.2°. The green vector in Fig. 4b thus signals a 41.8° increase (180° – 138.2°) in dihedral angle about edge 12 from its tail at the 566 end on the right to its head at the 666 end on the left, a dihedral angle discrepancy (DAD).

As shown in stereo Fig. 4d, to accommodate the green DAD, the large dihedral angle (180°) at the (666) head of the green DAD holds the *a* and *a′* edges down, whereas the smaller dihedral angle (138.2°) at the (566) tail of the green DAD raises the *c* and *c′* edges up.

A red vector (from a 556 vertex to a 566 vertex) codes an 18.4° DAD (Fig. 4b), and a blue vector (from a 555 vertex to a 556 vertex) codes a 14.6° DAD (Fig. 4b). Although the magnitudes of the red and blue DADs are smaller than the 41.8° of the green DADs, the red and blue DADs distort one and two

side pentagons, respectively, which are less accommodating than hexagons.

The Rule

The Rule excludes self assembly or persistence of cages with faces that would be severely nonplanar. The physical mechanism of the Rule acts at the level of the Ring, a center (pentagonal or hexagonal) face and its (five or six) external faces.[20] Several of these are illustrated in Fig. 4a. Given the types (hexagon or pentagon) of all of the faces external to a (center) face, the nature of every edge of the center face—green, red, blue, or no DAD—is fully determined.[19]

There are 13 hexagon-centered rings (hex-rings) and eight pentagon-centered Rings (pent-rings).[19] For some rings, like hex-ring 633 in Fig. 4a, none of the edges of the center face has a DAD. The external faces of these rings are unstressed, so these rings would readily self assemble.

For the center face of other Rings, like hex-ring 611 in Fig. 4a, some of the edges have a DAD, but these DAD vectors are not in a head-to-tail arrangement. As explained elsewhere,[20] and as denoted by the long, curved green arrow for hex-Ring 611, Rings of this sort can share the rotation of external edges due to the green DAD, partly from edge *e* to edge *c* in the face external to that green DAD edge, and partly from edge *c* to edge *a* in the neighboring external face. (Equation 8 in Ref. 20 shows that the sum of the rotations of external edges (e.g., edge *e* to edge *c* and edge *c* to edge *a*) in one of the symmetric halves of a Ring is equal to minus the sum of the DADs in that half.) The external faces in these Rings are only moderately nonplanar, so these Rings would also self assemble.

By contrast, when DADs are arranged head-to-tail, as they are in hex-Ring 631 in Fig. 4a, each DAD causes an external rotation that cannot be shared.[20] The red DAD would cause rotation of edge *e* to edge *c* about edge *d* by the full amount (18.4°) of the red DAD, as denoted by the curved red arrow. The green DAD would cause rotation of edge *c* to edge *a* about edge *b* by the full amount (41.8°) of the green DAD, as denoted by the curved green arrow. As a result, the faces external to both the red and the green DAD edges would be severely nonplanar. For example, as shown in Fig. 4f, sighting down edge *b* in hex-Ring 631 shows the severe nonplanarity of the hexagon external to the edge with the green DAD. If a Ring with head-to-tail DADs could self assemble, those nonplanar external faces would be greatly stressed. Thus, hex-Ring 631 would be unlikely to assemble in the first place or would be unlikely to persist.

The weak version of the Rule

Hex-Ring 631 (Fig. 4a) has two sets of head-to-tail DADs, one on each side of the Ring. So do two other hex-Rings and two pent-Rings, including 521 (Fig. 4a). However, hex-Ring 632 (Fig. 4a) has just one set. The Rule predicts that no cage with any of the six improbable Rings—the four hex-Rings and two pent-Rings with head-to-tail DADs—would self assemble. With just one set of head-to-tail DADs, however, hex-Ring 632 might be not quite so improbable, so a weak version of the Rule predicts that cages with the 632 hex-Ring but none of the other five improbable Rings might self assemble.[19]

Acknowledgements

I thank Yifan Cheng, Werner Boll, Tomas Kirchhausen, Stephen Harrison and Thomas Walz, the authors of Ref. 23, for providing me with a version of their Fig. 4B without the occluding vesicles. I thank Franklin Krasne for assistance with the text.

References

1. Kanaeseki, T. & Kadota, K. (1969). The "vesicle in a basket." A morphological study of the coated vesicle isolated from the nerve endings of the guinea pig brain, with special reference to the mechanism of membrane movements. *J. Cell Biol.* **42**, 202–220.
2. Pearse, B. M. F. (1975). Coated vesicles from pig brain: purification and biochemical characterisation. *J. Mol. Biol.* **97**, 93–98.
3. Crowther, R. A. & Pearse, B. M. F. (1981). Assembly and packing of clathrin into coats. *J. Cell Biol.* **91**, 790–797.
4. Pearse, B. M. F. (1976). Clathrin: a unique protein associated with intracellular transfer of membrane by coated vesicles. *Proc. Natl Acad. Sci. USA*, **73**, 1255–1259.
5. Ungewickell, E. & Branton, D. (1981). Assembly units of clathrin coats. *Nature*, **289**, 420–422.
6. Kirchhausen, T. & Harrison, S. C. (1981). Protein organization in clathrin trimers. *Cell*, **23**, 755–761.
7. Brodsky, F. M., Chen, C. Y., Knuehl, C., Towler, M. C. & Wakeham, D. E. (2001). Biological basket weaving: formation and function of clathrin-coated vesicles. *Annu. Rev. Cell Dev. Biol.* **17**, 517–568.
8. Ehrlich, M., Boll, W., Van Oijen, A., Hariharan, R., Chandran, K., Nibert, M. L. & Kirchhausen, T. (2004). Endocytosis by random initiation and stabilization of clathrin-coated pits. *Cell*, **118**, 591–605.
9. Fowler, P. W. & Manolopoulos, D. E. (1995). *An Atlas of Fullerenes.* Clarendon Press, Oxford.
10. Crowther, R. A., Finch, J. T. & Pearse, B. M. F. (1976). On the structure of coated vesicles. *J. Mol. Biol.* **103**, 785–798.
11. Kroto, H. W., Heath, J. R., O'Brien, S. C., Curl, R. F. & Smalley, R. E. (1985). C_{60}: buckminsterfullerene. *Nature*, **318**, 162–163.
12. Krätschmer, W., Lamb, L. D., Fostiropoulos, K. & Huffman, D. R. (1990). Solid C_{60}: a new form of carbon. *Nature*, **347**, 354–358.
13. Kroto, H. W. (1987). The stability of the fullerenes C_n (n = 24, 28, 32, 50, 60 and 70). *Nature*, **329**, 529–531.
14. Schmalz, T. G., Seitz, W. A., Klein, D. J. & Hite, G. E. (1988). Elemental carbon cages. *J. Amer. Chem. Soc.* **110**, 1113–1127.
15. Taylor, R., Hare, J. P., Abdul-Sada, A. K. & Kroto, H. W. (1990). Isolation, separation and characterisation of the fullerenes C_{60} and C_{70}: The third form of carbon. *J. Chem. Soc. Chem. Commun.* **1990**, 1423–1425.

16. Kikuchi, K., Nakahara, N., Wakabayashi, T., Honda, M., Matsumiya, H., Moriwaki, T., Achiba, Y. *et al.* (1992). Isolation and identification of fullerene family: C_{76}, C_{78}, C_{82}, C_{84}, C_{90} and C_{96}. *Chem. Phys. Lett.* **180**, 177–180.
17. Thilgen, C. & Diederich, F. (2006). Structural aspects of fullerene chemistry – a journey through fullerene chirality. *Chem. Rev.* **106**, 5049–5135.
18. Piskoti, C., Yarger, J. & Zettl, A. (1998). C_{36}, a new carbon solid. *Nature*, **393**, 771–774.
19. Schein, S. & Sands-Kidner, M. (2008). A geometric principle may guide self assembly of fullerene cages from clathrin triskelia and from carbon atoms. *Biophys. J.* **94**, 958–976.
20. Schein, S., Sands-Kidner, M. & Friedrich, T. (2008). The physical basis for the head-to-tail rule that excludes most fullerene cages from self assembly. *Biophys. J.* **94**, 938–957.
21. Manolopoulos, D. E., May, J. C. & Down, S. E. (1991). Theoretical studies of the fullerenes: C_{34} to C_{70}. *Chem. Phys. Lett.* **181**, 105–111.
22. Schein, S. & Friedrich, T. (2008). A geometric constraint, the head-to-tail exclusion rule, may be the basis for the isolated-pentagon rule (IPR) in fullerenes with more than 60 vertices. *Proc. Natl Aacd. Sci. USA*, **105**, 19142–19147.
23. Cheng, Y., Boll, W., Kirchhausen, T., Harrison, S. C. & Walz, T. (2007). Cryo-electron tomography of clathrin-coated vesicles: structural implications for coat assembly. *J. Mol. Biol.* **365**, 892–899.
24. Brinkmann, G., Friedrichs, O. D., Dress, A. & Harmuth, T. (1997). CaGe—a virtual environment for studying some special classes of large molecules. *Match*, **36**, 233–237.
25. Crick, F. H. C. & Watson, J. D. (1956). The structure of small viruses. *Nature*, **177**, 473–475.
26. Caspar, D. L. D. & Klug, A. (1962). Physical principles in the construction of regular viruses. *Cold Spring Harbor Symp. Quant. Biol.* **27**, 1–24.
27. Baker, T. S., Olson, N. H. & Fuller, S. D. (1999). Adding the third dimension to virus life cycles: three-dimensional reconstruction of icosahedral viruses from cryo-electron micrographs. *Microbiol. Mol. Biol. Rev.* **63**, 862–922.
28. Crowther, R. A. & Pearse, B. M. F. (1981). Assembly and packing of clathrin into coats. *J. Cell Biol.* **91**, 790–797.
29. Greene, B., Liu, S. -H., Wilde, A. & Brodsky, F. M. (2000). Complete reconstitution of clathrin basket formation with recombinant protein fragments: adaptor control of clathrin self assembly. *Traffic*, **1**, 69–75.
30. Handschuh, H., Ganteför, G., Kessler, B., Bechthold, P. S. & Eberhardt, W. (1995). Stable configurations of carbon clusters: chains, rings, and fullerenes. *Phys. Rev. Lett.* **74**, 1095–1098.
31. Kietzman, H., Rochow, R., Ganteför, G., Eberhardt, W., Vietze, K., Seifert, G. & Fowler, P. W. (1998). Electronic structure of small fullerenes: evidence for the high stability of C_{32}. *Phys. Rev. Lett.* **81**, 5378–5381.
32. O'Brien, S. C., Heath, J. R., Curl, R. F. & Smalley, R. E. (1988). Photophysics of buckminsterfullerene and other carbon cluster ions. *J. Chem. Phys.* **88**, 220–230.
33. Smalley, R. E. (1992). Fullerene self assembly. *Accts Chem. Res.* **25**, 98–105.
34. Zheng, G., Irle, S. & Morokuma (2005). Towards formation of buckminsterfullerene C_{60} in quantum chemical molecular dynamics. *J. Chem. Phys.* **122**, 014708–1–014708-7.
35. Irle, S., Zheng, G., Wang, Z. & Morokuma, K. (2006). The C_{60} formation puzzle "solved": QM/MD simulations reveal the shrinking hot giant road of the dynamic fullerene self-assembly mechanism. *Phys. Chem. B*, **110**, 14531–14545.
36. Huang, J. Y., Ding, F., Jiao, K. & Yakobson, B. I. (2007). Real time microscopy, kinetics, and mechanism of giant fullerene evaporation. *Phys. Rev. Lett.* **99**, 175503–1–175503-4.
37. Curl, R. F., Lee, M. K. & Scuseria, G. E. (2008). C_{60} buckminsterfullerene high yields unraveled. *J. Phys. Chem. A*, **112**, 11951–11955.
38. Zaremba, S. & Keen, J. H. (1983). Assembly polypeptides from coated vesicles mediate reassembly of unique clathrin coats. *J. Cell Biol.* **97**, 1339–1347.
39. Jin, A. J. & Nossal, R. (1993). Topological mechanisms involved in the formation of the clathrin coated vesicles. *Biophys. J.* **65**, 1523–1537.
40. Mashl, R. J. & Bruinsma, R. F. (1998). Spontaneous-curvature theory of clathrin-coated membranes. *Biophys. J.* **74**, 2862–2875.
41. Nossal, R. (2001). Energetics of clathrin basket assembly. *Traffic*, **2**, 138–147.
42. Wakeham, D. E., Chen, C.-Y., Greene, B., Hwang, P. K. & Brodsky, F. M. (2003). Clathrin self-assembly involves coordinated weak interactions favorable for cellular regulation. *EMBO J.* **22**, 4980–4990.
43. Fotin, A., Cheng, Y., Sliz, P., Grigorieff, N., Harrison, S. C., Kirchhausen, T. & Walz, T. (2004). Molecular model for a complete clathrin lattice from electron cryomicroscopy. *Nature*, **432**, 573–579.
44. Wu, X., Zhao, X., Baylor, L., Kaushal, S., Eisenberg, E. & Greene, L. E. (2001). Clathrin exchange during clathrin-mediated endocytosis. *J. Cell Biol.* **155**, 291–300.
45. Wu, X., Zhao, X., Puertollano, R., Bonifacino, J. S., Eisenberg, E. & Greene, L. E. (2003). Adaptor and clathrin exchange at the plasma membrane and trans-Golgi network. *Mol. Biol. Cell*, **14**, 516–528.
46. Yim, Y. -I., Scarselletta, S., Zang, F., Xufeng, W., Lee, D. -W., Kang, Y., Greene, L. E. *et al.* (2005). Exchange of clathrin, AP2 and epsin on clathrin-coated pits in permeabilized tissue culture cells. *J. Cell Sci.* **118**, 2405–2413.
47. Curl, R. F. (1993). On the formation of the fullerenes. *Phil. Trans. Phys. Sci. Eng.* **343**, 19–32.
48. Heath, J. R. (1991). Synthesis of C60 from small carbon clusters: a model based on experiment and theory. In *Fullerenes: Synthesis, Properties, and Chemistry of Large Carbon Clusters ACS Symp. ser 481* (Hammond, G. S. & Kuck, V. J., eds), pp. 1–23, American Chemical Society, Washington, D.C.